Coupling photocatalytic water oxidation with organic reduction: strategy for using water to reduce organic molecules

Xinzhe Tian
Henan Agricultural University
Yinggang Guo
Henan Agricultural University
Wenbo Liu
Henan Agricultural University
Yi Zheng
Henan Agricultural University
Yun-Lai Ren (renyunlai@126.com)
Henan Agricultural University https://orcid.org/0000-0002-5605-5137
Wankai An
Henan Agricultural University
Caoyuan Niu
Henan Agricultural University
Jianji Wang
Henan Normal University

Article

Keywords: photocatalysis, green chemistry, aryl bromides

Posted Date: September 11th, 2021

DOI: https://doi.org/10.21203/rs.3.rs-877546/v1

Version of Record: A version of this preprint was published at Nature Communications on October 19th, 2022. See the published version at https://doi.org/10.1038/s41467-022-33778-9.

Coupling photocatalytic water oxidation with organic reduction: strategy for using water to reduce organic molecules

Xinzhe Tian,[1] Yinggang Guo,[1] Wenbo Liu,[1] Yi Zheng,[1] Yun-Lai Ren,[1,*] Wankai An,[1] Caoyuan Niu,[1] Jianji Wang[2]*

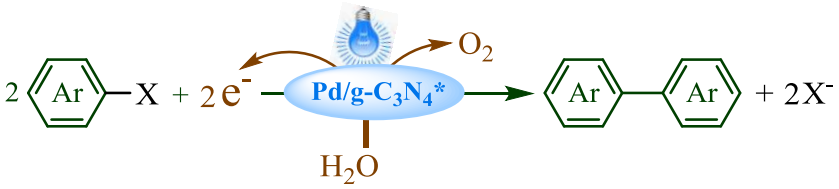

The utilization of readily available and non-toxic water by photocatalytic water splitting is highly attractive in green chemistry. Herein we report that light-induced oxidative half-reaction of water splitting is effectively coupled with reduction of organic compounds, which opens up, for the first time, an avenue to use water as an electron donor to enable reductive transformations of organic substances. The used photocatalyst (Pd/g-C_3N_4*) was synthetized by a novel method where Pd/g-C_3N_4 was irradiated by light in the presence of Na_2CO_3 and H_2O. The present strategy allowed a series of aryl bromides to undergo the reductive coupling to provide biaryl products in low to high yields. Preliminary mechanistic investigation suggests that the reaction proceeds through the single electron transfer from Pd to aryl bromides. This work will guide chemists to use water as a reducing agent to develop clean procedures for various organic reactions.

[1] College of Science, Henan Agricultural University, Zhengzhou, Henan 450002, P.R. China. Xinzhe Tian, Yinggang Guo, Wenbo Liu and Yi Zheng contributed equally to this work. [2] School of Chemistry and Chemical Engineering, Henan Normal University, Xinxiang, Henan 453007, P. R. China. Correspondence and requests for materials should be addressed to Yun-Lai Ren (email: renyunlai@126.com) or to Jianji Wang (email: Jwang@htu.cn).

Utilization of water is considerably attractive in green chemistry due to its readily available, non-toxic and non-flammable features[1-3]. As a result, much attention has been devoted to applications of water in various fields, e.g. organic reactions with water as the solvent[4-10], hydrogen production by water splitting[11-28] and so on[29,30]. Recently, several novel uses of water in organic synthesis have been developed via the challenging photocatalytic water splitting. As shown in Fig. 1a, the first kind is the utilization of water as the oxygen source for oxygenation of organic molecules by coupling the oxygenation with light-induced water oxidation half-reaction[31-34], in which the oxidants such as $[Co^{III}(NH_3)_5Cl]^{2+}$and $(NH_4)_2Ce(NO_3)_6$ have been added as the electron acceptor[31,32]. Subsequently, additional oxidant-free methods[33,34] have been developed for oxygenation of olefin and benzene C−H bonds by coupling the oxygenation with the two half-reactions of the photocatalytic water splitting (Fig. 1a). The second kind is the proton reduction half-reaction coupled with oxidation of organic compounds (Fig. 1b)[35-40], and has provided a strategy for oxidative transformations of alcohols[35-38], thiols[39], and benzylamines[40]. The third kind is that the proton reduction half-reaction is coupled with the hydrogenation (Fig. 1c)[41-46], showing a use of water as the hydrogen source for the hydrogenation of olefins, nitro compounds, aldehydes and halogenated compounds, in which the reducing agents such as metal powders, triethanolamine, ammonium oxalate, Na_2SO_3 and so on have been added to reduce H_2O to hydrogen. Similar methods have also been applied in deuteration of halogenated compounds with D_2O[45,46].

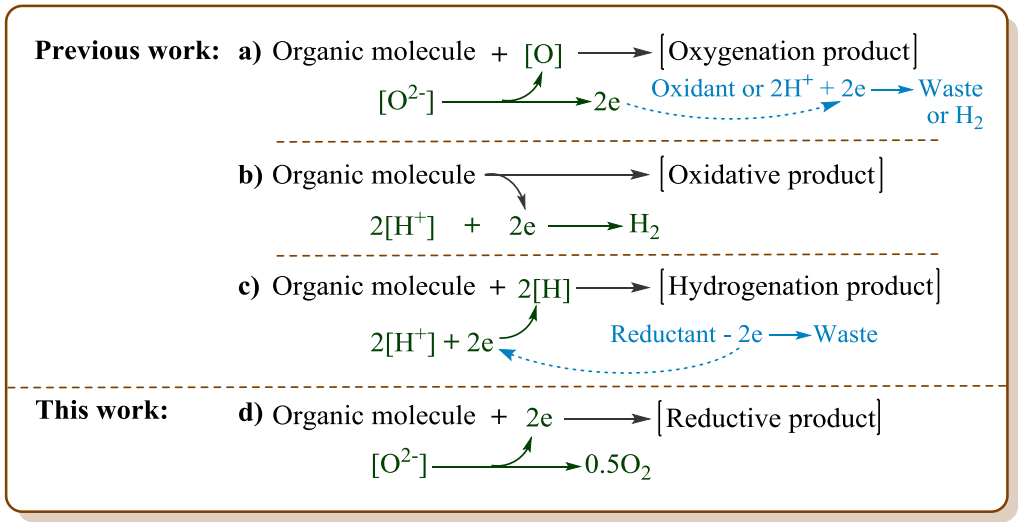

Fig. 1 Coupling organic reactions with photocatalytic half-reaction of water splitting

To the best of our knowledge, there is no report related to coupling photocatalytic water oxidation half-reaction with the reduction of organic compounds (Fig. 1d). However, it is desired to overcome this problem because a new use of water as the green reducing agent to enable the reductive transformations of organic substances can be developed by this way. In addition, the reductive coupling of aryl or alkyl halides is of great significance in modern organic synthesis[47-56], which has prompted us to select this kind of reaction as the model reaction to make our idea come true. Encouraged by prior success in applying carbon nitride-supported transition metal (M/g-C_3N_4) into photocatalytic water splitting,[57-65] we selected this kind of semiconductor to achieve our goals. It is worth noting that the proton reduction is desired in previous literatures related to M/g-C_3N_4-catalyzed water splitting, while this half-reaction would inhibit our reaction[44-46,57-65]. Therefore, the M/g-C_3N_4 and reaction conditions had to be modified to accelerate the water oxidation and inhibit the proton reduction via a new method, and the results are herein reported.

Results and discussion

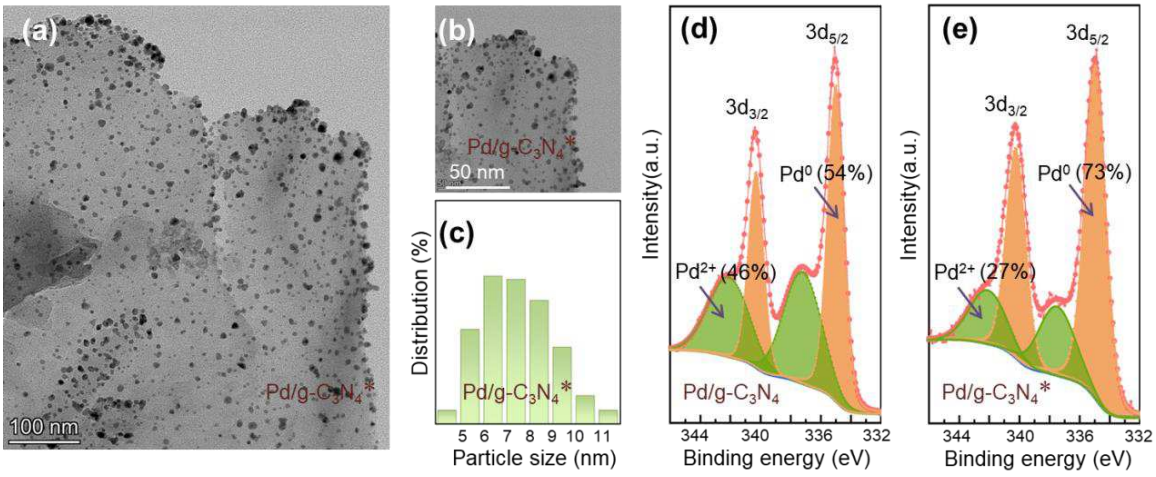

Fig. 2 The samples of 3 wt% Pd/g-C_3N_4 and 3 wt% Pd/g-C_3N_4* (a) TEM image, (b) TEM image, (c) size distribution of Pd nanoparticles, (d) Pd 3d XPS spectrum, (e) Pd 3d XPS spectrum.

Preparation and characterization of photocatalyst. Graphitic carbon nitride (g-C_3N_4) nanosheets were prepared by the exfoliation of bulk g-C_3N_4 under an assistance of water[44], which was followed by the preparation of transition metal/g-C_3N_4 via a thermal reduction method using g-C_3N_4 nanosheets and the transition metal in an oxidized state[44]. In order to improve the catalytic activity, Pd/g-C_3N_4 was irradiated by the blue light in the presence of

Na_2CO_3 and H_2O to give the activated Pd/g-C_3N_4 (named as Pd/g-C_3N_4*). The synthesized catalysts were characterized via the transmission electron microscope (TEM). According to the TEM image, the Pd nanoparticles in Pd/g-C_3N_4* are uniformly dispersed (Fig. 2a and 2b), and has a narrow size distribution in the range of 5-10 nm (Fig. 2c). In addition, we examined the chemical state of Pd by X-ray photoelectron spectroscopy (XPS). As shown in Fig. 2d and 2e, the deconvoluted peaks related to the $3d_{3/2}$ and $3d_{5/2}$ orbitals of Pd^0 are 340.23 and 335.00 eV[66], while another two shoulder peaks should be assigned to Pd^{2+}. Based on the area of the peaks, the percentage of Pd^0 in the Pd nanoparticles in two cases are 54% and 73%, respectively, which indicates that our activating treatment method can increase the percentage of Pd^0.

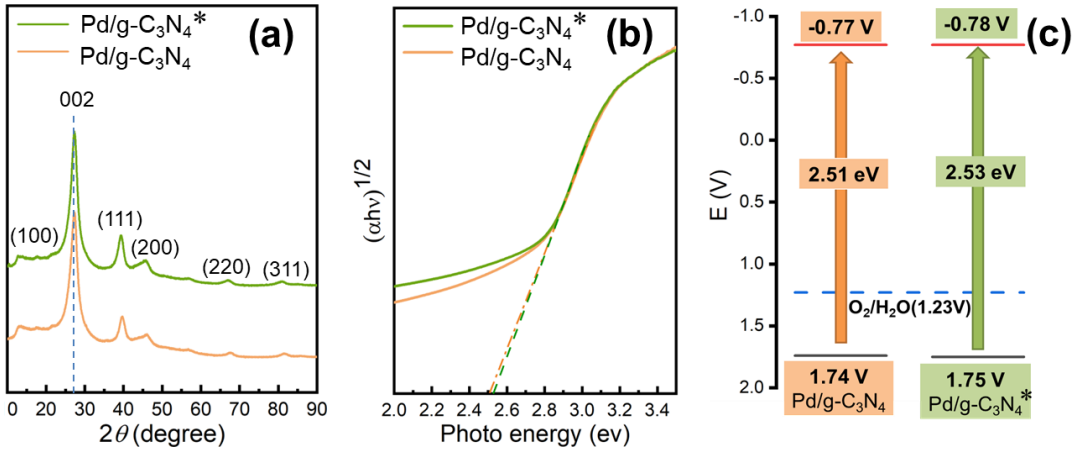

Fig. 3 Samples of 3 wt% Pd/g-C_3N_4 and 3 wt% Pd/g-C_3N_4*: (a) X-ray diffraction patterns, (b) Kubelka–Munk plots, (c) Energy-band positions.

As seen from X-ray diffraction patterns (Fig. 3a), the diffraction peak from Pd had change little when Pd/g-C_3N_4 was activated by our method, which reveals that the activating treatment would not result in significant leaching losses of Pd nanoparticles. Next, we investigated the photoelectro-chemical characteristics of the two catalysts. The results from the calculation via the Kubelka–Munk function show that the optical band gaps (Eg) of Pd/g-C_3N_4 and Pd/g-C_3N_4* are 2.51eV and 2.53 eV, respectively (Fig. 3b). The conduction band positions (Ec) vs. standard calomel electrode (SCE) were also clarified via the cyclic voltammetric curves, and the results show that the Ec in two cases are -0.77 V and -0.78 V, respectively (see Fig. 3c). Thus the valence band positions (Ev) in two cases can be estimated to be 1.74 V and 1.75 V, respectively (see Fig. 3c). These results reveal that the electronic

band structure of the present semiconductor catalyst has change little after our activating treatment.

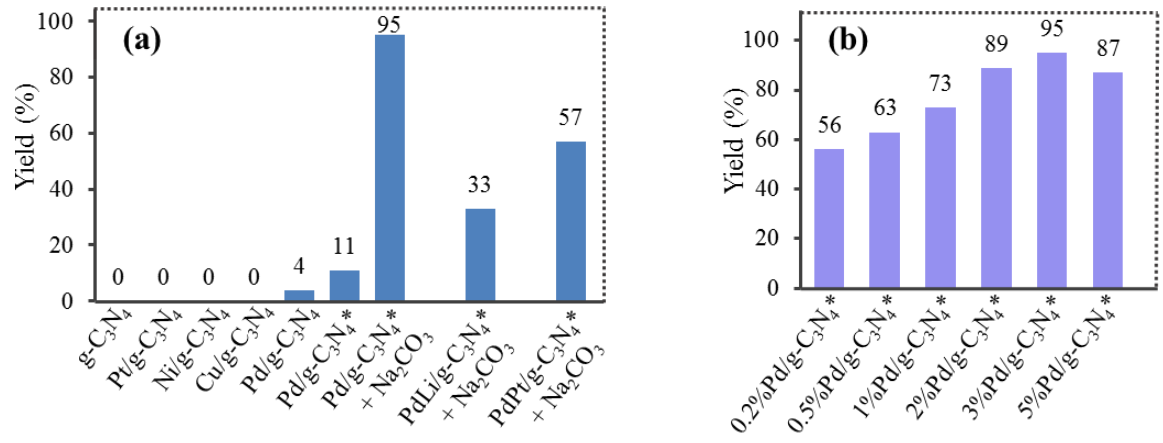

Fig. 4 Reductive coupling of bromobenzene with various catalysts under the conditions: 0.5 mmol bromobenzene, 15 mg M/g-C_3N_4, 5 mL H_2O, 3 mL 1,4-dioxane, Ar atmosphere, light source: 420 nm LED, 75 W. Pd/g-C_3N_4*: the activated Pd/g-C_3N_4 via our method. 1.5 equiv Na_2CO_3 was added in the last three experiments shown in Fig 4a. In all cases of Fig 4a, the loading of the transition metal on g-C_3N_4 was 3 wt%. In all cases of Fig 4b, 1.5 equiv Na_2CO_3 was added, and x%Pd/g-C_3N_4* means that the loading of Pd in Pd/g-C_3N_4* is x wt%.

Effect of various conditions on the reductive coupling of bromobenzene. Reductive coupling of bromobenzene was chosen as the model reaction to search for suitable photocatalysts under blue light (420 nm). As shown in Fig. 4a, the reductive coupling did not occur in the case of bare g-C_3N_4 nanosheet, while the deposition of 3 wt% Pd on g-C_3N_4 gave the biphenyl product in 4% yield, suggesting that the Pd species played a role of the catalytic sites. Other transition metals including Pt, Ni and Cu supported on g-C_3N_4 were also test, but no targeted product was observed. In order to obtain a good result, we had to modify the photocatalyst, and found that the yield increased from 4% to 11% when Pd/g-C_3N_4 was irradiated for 5 min in the presence of Na_2CO_3 and water. These results indicate that the irradiating process can enhance the catalytic ability of Pd/g-C_3N_4, which is possibly due to that Pd^0 is the catalytically active species[47-49], and such a process can result in an increase in the ratio of Pd^0 to Pd^{2+} based on the characterization of catalyst. In addition, we observed the formation of hydrogen gas from the proton reduction that was unbeneficial for the reductive coupling, urging us to add a base to inhibit this competing reaction. Indeed, the biphenyl product was obtained in as high as 95% yield in the presence of Na_2CO_3. PdLi/g-C_3N_4* and PdPt/g-C_3N_4* were also examined as the catalysts, but the targeted product was obtained in

only 33% and 57% yields, respectively. Subsequently, an effect of the Pd loading amount on the reaction was investigated, and the results in Fig. 4b show that 3 wt% Pd loading is optimum. The yield significantly dropped with decreasing the Pd loading from 3 wt%. However, when the Pd loading increased to 5 wt% from 3 wt%, a lower yield was obtained, which is possibly rationalized by assuming that the aggregation of excess Pd nanoparticles would lead to the charge recombination[44].

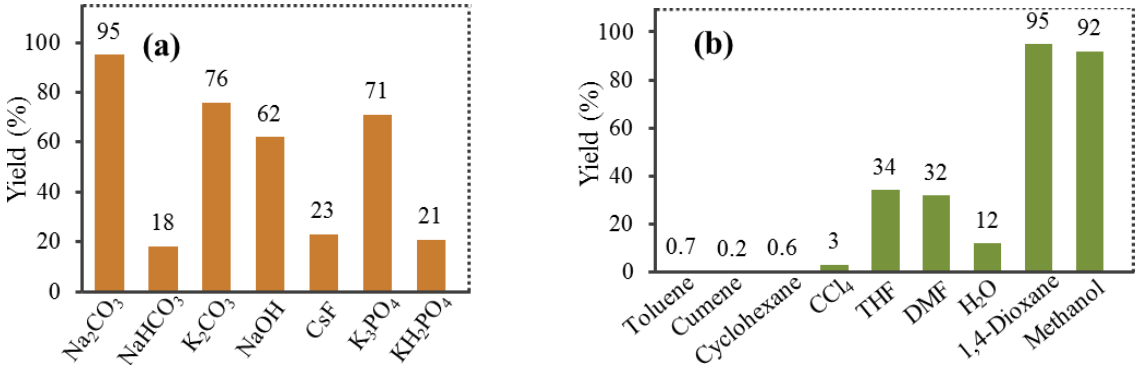

Fig. 5 Reductive coupling of bromobenzene with various bases and solvents under the conditions: 0.5 mmol bromobenzene, 15 mg Pd/g-C_3N_4* (3 wt% Pd), 1.5 equiv base, 5 mL H_2O, 3 mL solvent, Ar atmosphere, light source: 420 nm LED, 75 W).

Among the screened bases, Na_2CO_3 turned out to be the most effective one (Fig. 5a). The targeted product was obtained in very low yields in the case of more weakly alkaline $NaHCO_3$ and KH_2PO_4, while the use of Na_2CO_3, K_2CO_3, K_3PO_4 or NaOH allowed the reaction to proceed smoothly with 62-95% yields. These results indicate that the basicity has an important effect on the reaction, most likely owing to that the presence of the base not only inhibits the H^+ reduction by decreasing the concentration of H^+, but also helps to produce the catalytically active Pd^0 species[47-49]. The reaction was highly dependent on the solvent type. The solvents including toluene, cumene, cyclohexane and CCl_4 were less effective, possibly due to the poor dispersion of the catalyst in these solvents based on our observation. On the contrary, the catalyst could be effectively dispersed in 1,4-dioxane and methanol, which allowed the reductive coupling to proceed smoothly.

Substrates scope exploration for the reductive coupling. With the optimized results in hand, we set out to evaluate the scope and generality of the reductive coupling with various aryl bromides. As shown in Table 1, a series of bromobenzenes underwent the reductive coupling

smoothly to give the targeted products in low to high yields (**2a**–**2o**). Moreover, the present method was compatible with various groups, e.g. cyano, carbonyl, ester, fluoro, chloro, alkyl, alkoxy, *N*,*N*-dimethylamino and hydroxy groups (**2b**–**2o**), even the highly reactive aldehyde group was also tolerated (**2c**). The electronic effect of substituents had an important effect on the reaction. Many bromobenzenes with electron-withdrawing groups were converted to the targeted products in high yields under 420 nm light (**2b**–**2g**), whereas such condition did not allow the substrates with strongly electron-donating groups to be smoothly converted (**2i**–**2k**). For instance, as high as 93% yield was obtained in the case of 4-bromobenzaldehyde (**1c**), while the reaction with 1,2-(methylenedioxy)-4-bromobenzene gave **2j** in only 28% yield under 420 nm light. Thus we had to change reaction conditions, and it was found that a use of

Table 1. Reductive coupling of various ary halides.[a]

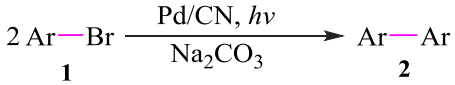

1 **2**

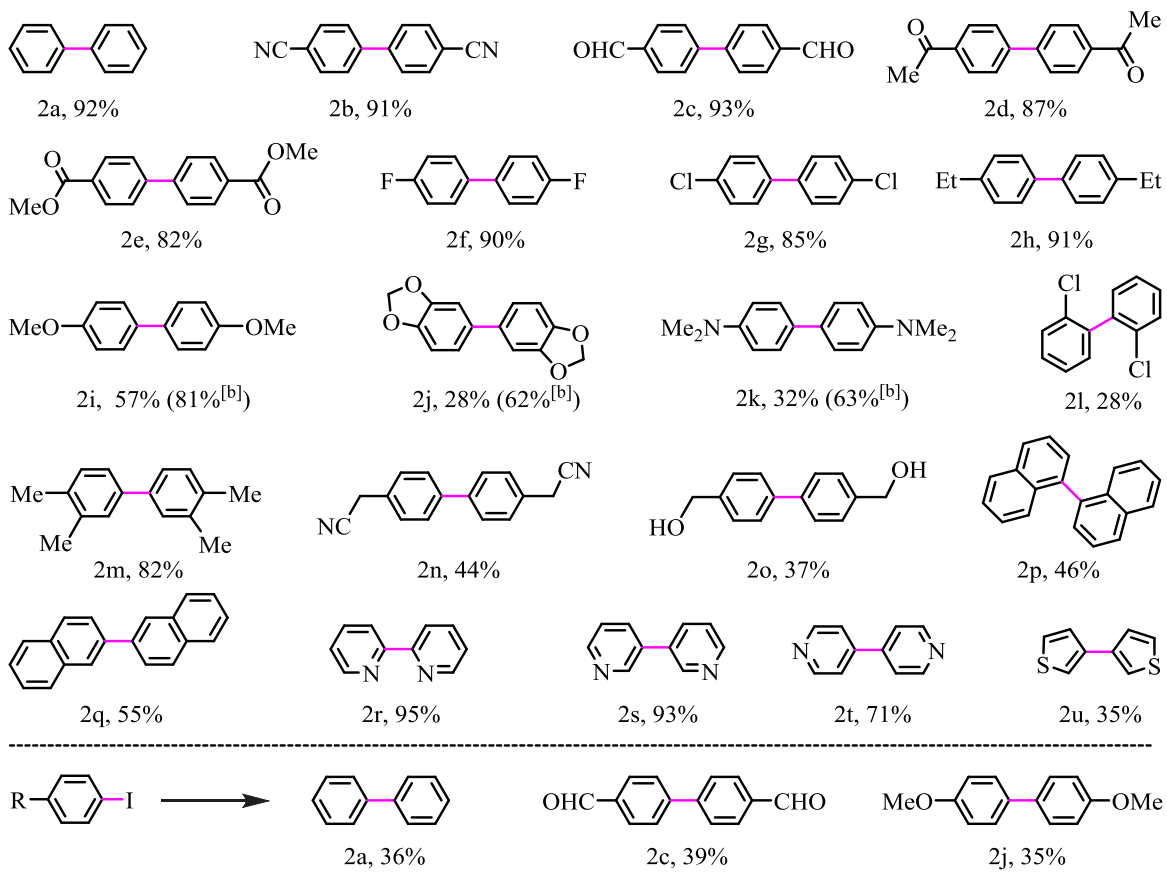

[a] Reaction conditions: 0.5 mmol aryl halides, 15 mg Pd/g-C_3N_4* (3 wt% Pd), 1.5 equiv Na_2CO_3, 5 mL H_2O, 3 mL 1,4-dioxane, Ar atmosphere, light source: 420 nm LED, 75 W; [b] 365 nm LED.

365 nm light allowed **2j** to be obtained in a higher yield. The present reaction was susceptible to the steric hindrance. For example, the reaction of 4-bromochlorobenzene proceeded smoothly to provide **2g** in 85% yield, while only 28% yield was obtained in the case of 2-bromochlorobenzene (**1l**). When 4-bromobenzenemethanol was used as the substrate, **2o** was obtained in 37% yield, accompanied by 5% 4,4'-diformylbiphenyl byproduct, which suggests that benzyl alcohol can undergo the oxidative dehydrogenation under the present condition.

We had tried the conversion of bromonaphthalenes, and the reductive coupling of 1- and 2-bromonaphthalenes gave **2p** and **2q** in 46% and 55% yields, respectively. It was noteworthy that the two substrates did not undergo complete conversion even if the reaction time was prolonged to 40 h, possibly owing to their lower reactivity caused by the larger steric hindrance around the reaction sites. Other kind of good substrates were bromopyridines, among which 2- and 3-bromopyridines worked smoothly affording the product **2r** and **2s** in as high as 95% and 93% yield, respectively. By comparison, the electron-rich heteroaryl bromides including bromofuranes and bromothiophenes were less reactive. For example, 3-bromothiophene was converted to **2u** in only 35% yield. These results suggest that an increase in the electron density of the aromatic ring would decrease the reactivity of the substrates, agreeing with our observations above related to the substituent effect. Aryl chlorides were also evaluated under the present conditions, and only trace amount of coupling product was observed. Strangely, aryl iodides were less reactive than aryl bromides under our condition although the C-I bond is more easily to be activated than the C-Br bond[46]. For example, the substrates including iodobenzene, 2-iodobenzaldehyde and methoxyiodobenzene was converted to the product **2a**, **2c** and **2j** in 36%, 39% and 35% yield, respectively. Based on these results, we inferred that the resulting I^- from the reductive coupling of iodobenzenes would block the present reaction. Indeed, when 1 equiv KI was added to the reaction system related to the coupling of bromobenzene, the yield of **2a** was decreased from 92% to 69%.

Reaction mechanism for the reductive coupling. Several control experiments were performed to gain insight into the reaction mechanism. As shown in Fig. 7a and 7b, hardly any reductive coupling product was observed in the absence of water or Pd/g-C_3N_4*,

indicating that both water and Pd/g-C_3N_4* were indispensable for the reaction. The absence of 1,4-dioxane would lead to a poor dispersion of the catalyst in these solvents based on our observation, thus the reaction did not go well in the pure water (Fig. 7c), which reveals that 1,4-dioxane plays a role of the dispersant. The present transformation may be a thermal-dependent reaction because Pd catalysts are often used to enable the light-free reductive coupling[47-49]. To rule out this possibility, we performed the control experiments without irradiation, and the results in Fig. 7d suggest that the present transformation is a light-dependent reaction.

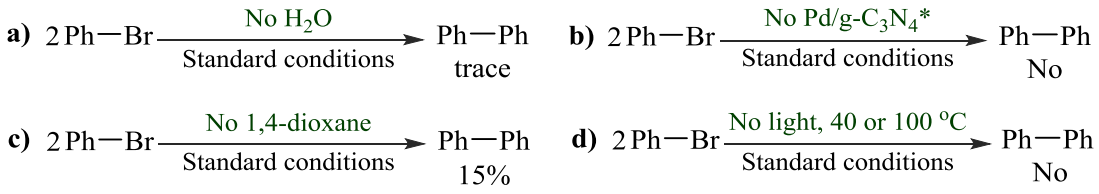

Fig. 7 Several control experiments (standard conditions: 0.5 mmol bromobenzene, 15 mg Pd/g-C_3N_4* (3 wt%), 1.5 equiv Na_2CO_3, 5 mL H_2O, 3 mL 1,4-dioxane, Ar atmosphere, light source: 420 nm LED, 75 W)

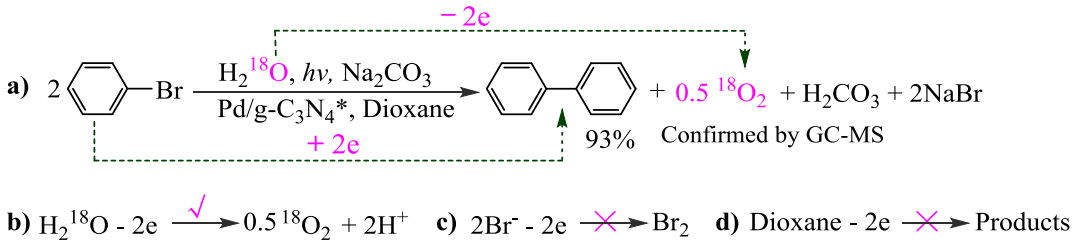

Fig. 8 Investigation on who is the electron donor

By all appearances, the present reactions undergo the coupling of two carbon atoms with a pronounced C^+ character to generate the C-C bond. Thus the presence of the reducing agent as the electron donor is required based on the conservation law of electric charge. We inferred that water served as the electron donor by the oxidation of H_2O molecule to O_2 under the present conditions. Indeed, the formation of $^{18}O_2$ was observed in the $H_2{}^{18}O$-labelling experiment where $H_2{}^{18}O$ was added into the reaction system (Fig. 8a and b). Maybe the resulting Br^- play the role of the electron donor via the conversion of Br^- to Br_2 (Fig. 8c), but this possibility was ruled out based on our experimental results: no Br_2 was detected after completion of the reaction. In addition, it is possible that dioxane or the benzene ring served as the electron donor by the oxidation of them (Fig. 8d). To rule out this possibility, we

analysed the reaction system after completion of the reaction using GC-MS and HPLC-MS, but no detectable amount of products from the oxidation of dioxane or the benzene ring was observed. Obviously, the experimental results above confirm the reliability of our conclusion that only water serves as the electron donor in the present reaction.

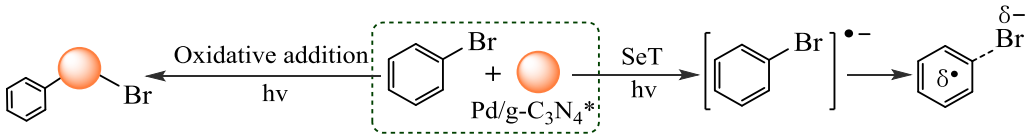

Fig. 9 Two kinds of mechanism pathways for the reductive coupling

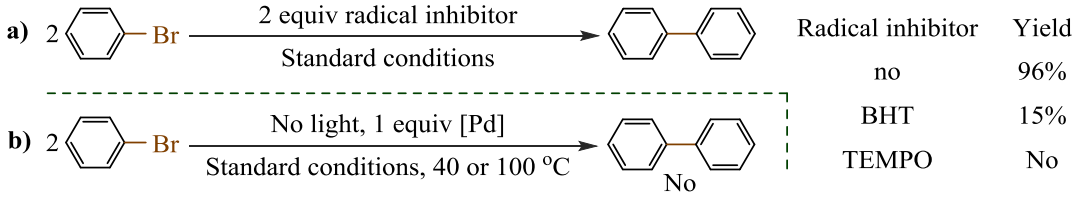

Fig. 10 Investigation on whether or not the coupling undergoes the single electron transfer (standard conditions: 0.5 mmol bromobenzene, 15 mg Pd/g-C_3N_4* (3 wt%), 1.5 equiv Na_2CO_3, 5 mL H_2O, 3 mL 1,4-dioxane, Ar atmosphere, light source: 420 nm LED, 75 W. The loading of Pd/g-C_3N_4* was changed to 1.77g in the case of Fig. 10b).

Two kinds of mechanisms for the reductive coupling of ary halides have been proposed in the previous literatures (Fig. 9). One undergoes the oxidative addition of ary halides to the transition metals[47-54]. The other starts with the formation of the aryl radical anion ($ArX^{\bullet -}$) by the single electron transfer (SeT) from catalysts to ary halides[45,46,56]. Considering that most of light-induced reductive coupling reactions of aryl halides undergo the SeT mechanism pathways[45,46,56], we guessed that the present reaction involved some free radicals. Indeed, the presence of the radical inhibitor 2,2,6,6-tetramethyl-1-piperidinyloxy (TEMPO) or 2,6-ditbutyl-4-methylphenol (BHT) would prevent the targeted product from being produced (Scheme 10a). However, only based on these results, we cannot affirm the present reaction undergoes the SeT pathway because that it is also possible that the radical inhibitors act as an electron-trapping agent to restrain the SeT from Pd to bromobenzene. According to previous literatures[47-49], the oxidative addition of aryl halides to the Pd^0 species can occur under thermal conditions, hence light-free conditions should allow the reductive coupling to proceed smoothly in the presence of stoichiometric Pd^0 species as the electron donor and the catalyst.

On the contrary, when 1 equiv Pd^0 species contained in the catalyst was used, the light-free reductive coupling of bromobenzene did not takes place at 100 °C, which suggests that the oxidative metal addition-based mechanism should be ruled out under our conditions.

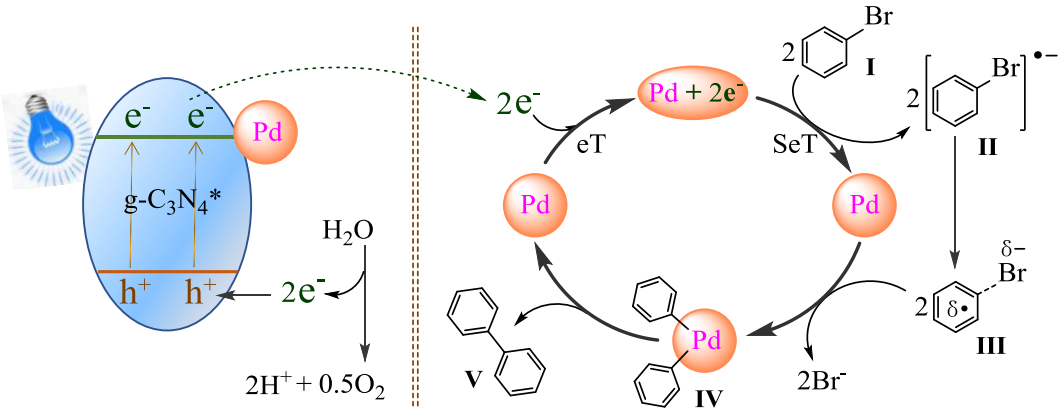

Fig. 11 Proposed mechanism for the photocatalytic reductive coupling using Pd/g-C_3N_4*.

Based on the observations above and previous literatures, a plausible mechanism pathway is proposed with the reductive coupling of bromobenzene as the representative. As shown in Fig. 11, g-C_3N_4 acts as the light absorber[64,65], and its electrons are excited from the valence band (VB) to the conduction band (CB) upon irradiation with light. On the one hand, the oxidation of H_2O to O_2 occurs at the VB via the electron transfer (eT) from O^{2-} of H_2O to the photogenerated holes under the assistance of Pd. On the other hand, the reductive coupling occurs at the CB of g-C_3N_4, and starts with the eT from g-C_3N_4 to Pd, followed by the SeT from Pd to bromobenzene **I** to produce intermediate **II** ($PhBr^{\bullet -}$) that can be converted to a phenyl radical-like species **III**[45,46,56]. Then the reaction between Pd and two molecules of the phenyl radical-like species provides diphenylpalladium **IV**. Finally, intermediate **IV** undergoes the reductive elimination to provide the targeted product **V**.

In conclusion, we report, for the first time, that water is used as the electron donor to enable the reductive transformations of organic substances by coupling the light-induced water oxidation half-reaction with the reduction of organic compounds in the presence of Pd/g-C_3N_4* photocatalyst, which is different from previous literatures[44-46,57-65] related to light--driven water splitting where the proton reduction half-reaction is desired to occur, while this half-reaction would inhibit our reactions. The used photocatalyst was synthetized by a novel method where previous Pd/g-C_3N_4 was irradiated by the light in the presence of

Na_2CO_3 and H_2O. Such an irradiating treatment can lead to an increase in the ratio of the catalytically active Pd^0 to Pd^{2+}, which is possibly the main reason why Pd/g-C_3N_4* is effective. The present strategy allowed a series of aryl bromides to undergo the reductive coupling to provide biaryl products in low to high yields under 420 nm blue LEDs. Preliminary mechanistic investigation suggests that the present reaction proceeds through the single electron transfer from the transition metals to aryl bromides. We believe that the present strategy will be also successfully applied to many reductive transformations of organic compounds with water as the reducing agent by changing the composition of the semiconductor photocatalyst.

Methods

Procedure for preparation of Pd/g-C_3N_4. Pd/g-C_3N_4 was prepared based on previous procedures in literatures[44,66]. After 50 mg g-C_3N_4 were added to a 100 mL flask equipped with 50 mL ethanol, the system was sonicated for 3 h to make g-C_3N_4 to be dispersed in ethanol. Then 100 mL K_2PdCl_6 solution (0.01M) was added and the mixture was stirred for 10 min. Subsequently, 5 mL of water was added and the mixture was refluxed at 90 ^oC for 1 h. Finally, the reaction mixture was cooled to room temperature, the precipitation was collected, washed with ethanol, dried at 60 ^oC under reduced pressure to give Pd/g-C_3N_4.

Procedure for preparation of Pd/g-C_3N_4*. 15.00 mg Pd/g-C_3N_4 and 79.50 mg Na_2CO_3 were added to a 10 mL quartz glass tube equipped with 5 mL H_2O, 3 mL 1,4-dioxane and a magnetic stirring under argon atmosphere. Then the reaction mixture was magnetically stirred for 5 min under 75 W blue LEDs. Once the reaction time was reached, the precipitate was filtrated and washed in turn with water and ethanol. The collected solid was dried at 80 ^oC under reduced pressure to give Pd/g-C_3N_4*.

General procedure for the reductive coupling. 15.00 mg Pd/g-C_3N_4 and 79.50 mg Na_2CO_3 were added to a 10 mL quartz glass tube equipped with 5 mL H_2O, 3 mL 1,4-dioxane and a magnetic stirring under argon atmosphere. After the reaction mixture was magnetically stirred for 5 min under blue LEDs (light source: 420 nm LED, 75 W) to give in-situ Pd/g-C_3N_4*, aryl bromide was added. Then the reaction tube was stirred magnetically to perform the reductive coupling for 20 h under 75 W blue LEDs (light source: 420 nm LED, 75 W) and argon flow.

Once the reaction time was reached, GC analysis of the mixture provided the GC yields of the product. Then the crude product from another parallel experiment was purified by silica gel chromatography to give the desired product.

Characterization. The photocatalysts were characterized by transmission electron microscope (TEM), X-ray photoelectron spectroscopy (XPS), X-ray diffraction patterns, UV-Vis spectroscopy. The reductive coupling products were confirmed by ^{1}H-NMR and ^{13}C-NMR spectra. The details of these techniques and the other experimental procedure were shown in the supplementary information.

Data availability

The authors declare that all other data supporting the findings of this study are included in this article and the supplementary information, or also available from the corresponding author upon reasonable request.

References

1. Sun, F. et al. Energy-saving hydrogen production by chlorine-free hybrid seawater splitting coupling hydrazine degradation. *Nat. Commun.* **12**, 4182, (2021).
2. Takata T. et al. Photocatalytic water splitting with a quantum efficiency of almost unity. *Nature* **581**, 411–414 (2020).
3. Ashida, Y., Arashiba, K., Nakajima, K. & Nishibayashi, Y. Molybdenum-catalysed ammonia production with samarium diiodide and alcohols or water. *Nature* **568**, 536–540 (2019).
4. Bailey, J. D. et al. Beyond organic solvents: synthesis of a 5-HT_4 receptor agonist in water. *Green Chem.* **23**, 788–795 (2021).
5. Meng, Q. L. et al. Sustainable production of benzene from lignin. *Nat. Commun.* **12**, 4534 (2021).
6. Kitanosono, T., Xu, P. Y. & Kobayashi, S. Chiral Lewis acids integrated withsingle-walled carbon nanotubes forasymmetric catalysis in water. *Science* **362**, 311–315 (2018).
7. Renders, T. et al. Catalytic lignocellulose biorefining in *n*-butanol/water: a one-pot approach toward phenolics, polyols, and cellulose. *Green Chem.* **20**, 4607–4619 (2018).
8. Cortes-Clerget, M. et al. Water as the reaction medium in organic chemistry: from our worst enemy to our best friend. *Chem. Sci.* **12**, 4237–4266 (2021).
9. Cortes-Clerget, M. et al. Bridging the gap between transition metal- and bio-catalysis via aqueous micellar catalysis. *Nat. Commun.* **10**, 2169 (2019).
10. Cortes-Clerget, M., Lee, N. R., Lipshutz, B. H. Synthetic chemistry in water: applications to peptide synthesis and nitro-group reductions. *Nat. Protoc.* **14**, 1108–1129 (2019).
11. Service, R. F. New electrolyzer splits water on the cheap. *Science* **367**, 1181–1181 (2020).
12. Liu, J. Metal-free efficient photocatalyst for stable visible water splitting via a two-electron pathway. *Science* **347**, 970–974 (2015).
13. Ye, S. et al. Unassisted photoelectrochemical cell with multimediator modulation for solar water

splitting exceeding 4% solar-to-hydrogen efficiency. *J. Am. Chem. Soc.* **143**, 12499−12508 (2021).
14. Ogawa, K. et al. Layered perovskite oxyiodide with narrow band gap and long lifetime carriers for water splitting Photocatalysis. *J. Am. Chem. Soc.* **143**, 8446−8453 (2021).
15. Ran, L. et al. Conformal macroporous inverse opal oxynitride-based photoanode for robust photoelectrochemical water splitting. *J. Am. Chem. Soc.* **143**, 7402−7413 (2021).
16. Chen, S. S. et al. Surface modifications of $(ZnSe)_{0.5}(CuGa_{2.5}Se_{4.25})_{0.5}$ to promote photocatalytic Z-scheme overall water splitting. *J. Am. Chem. Soc.* **143**, 10633−10641 (2021).
17. Zhai, P. L. et al. Engineering single-atomic ruthenium catalytic sites on defective nickel-iron layered double hydroxide for overall water splitting. *Nat. Commun.* **12**, 4587 (2021).
18. Yoon, K. Y. et al. $NiFeO_x$ decorated Ge-hematite/perovskite for an efficient water splitting system. *Nat. Commun.* **12**, 4309 (2021).
19. Yan, X. Y. et al. A membrane-free flow electrolyzer operating at high current density using earth-abundant catalysts for water splitting. *Nat. Commun.* **12**, 4143 (2021).
20. Huang, D. W. et al. Wittichenite semiconductor of Cu_3BiS_3 films for efficient hydrogen evolution from solar driven photoelectrochemical water splitting. *Nat. Commun.* **12**, 3795 (2021).
21. Ebihara, M. et al. Charge carrier mapping for Z-scheme photocatalytic water-splitting sheet via categorization of microscopic time-resolved image sequences. *Nat. Commun.* **12**, 3716 (2021).
22. 19 Ji, X. X. et al. Graphene/MoS_2/$FeCoNi(OH)_x$ and Graphene/MoS_2/$FeCoNiP_x$ multilayer-stacked vertical nanosheets on carbon fibers for highly efficient overall water splitting. *Nat. Commun.* **12**, 1380 (2021).
23. Wu D. S. et al. Efficient overall water splitting in acid with anisotropic metal nanosheets. *Nat. Commun.* **12**, 1145 (2021).
24. Wang Z. et al. Sequential cocatalyst decoration on $BaTaO_2N$ towards highly-active Z-scheme water splitting. *Nat. Commun.* **12**, 1005 (2021).
25. Sun, M. et al. Photo-driven oxygen vacancies extends charge carrier lifetime for efficient solar water splitting. *Angew. Chem. Int. Ed.* **60**, 17601–17607 (2021).
26. Sun, R. et al. Strain-engineered nano-ferroelectrics for high-efficiency piezocatalytic overall water splitting. *Angew. Chem. Int. Ed.* **60**, 16019–16026 (2021).
27. Zhu, J. W. et al. Regulative electronic states around ruthenium/ruthenium disulphide heterointerfaces for efficient water splitting in acidic media. *Angew. Chem. Int. Ed.* **60**, 12328–12334 (2021).
28. Li, M. G. et al. Exclusive strain effect boosts overall water splitting in PdCu/Ir core/shell nanocrystals. *Angew. Chem. Int. Ed.* **60**, 8243 –8250 (2021).
29. Wen F. et al. Amide-bridged conjugated organic polymers: efficient metal-free catalysts for visible-light driven CO_2 reduction with H_2O to CO. *Chem. Sci.* **12**, 11548–11553 (2021).
30. Wu, Y. M. et al. Selective Transfer Semihydrogenation of Alkynes with H_2O (D_2O) as the H (D) Source over a Pd-P Cathode. *Angew. Chem. Int. Ed.* **59**, 21170–21175 (2020).
31. Hirai, Y. et al. Ruthenium-catalyzed selective and efficient oxygenation of hydrocarbons with water as an oxygen source. *Angew. Chem. Int. Ed.* **47**, 5772–5776 (2008).
32. Fukuzumi, S., Kishi, T., Kotani, H., Lee, Y.-M. & Nam, W. Highly efficient photocatalytic oxygenation reactions using water as an oxygen source. *Nat. Chem.* **3**, 38–41, (2011).
33. Singh, W. M. et al. Hydrogen production coupled to hydrocarbon oxygenation from photocatalytic water splitting. *Angew. Chem. Int. Ed.* **51**, 1653–1656 (2012).
34. Zheng, Y.-W. et al. Photocatalytic hydrogen-evolution cross-couplings: Benzene C−H amination and

hydroxylation. *J. Am. Chem. Soc.* **138**, 10080−10083 (2016).
35. Kasap, H. et al. Solar-driven reduction of aqueous protons coupled to selective alcohol oxidation with a carbon nitride−molecular Ni catalyst system. *J. Am. Chem. Soc.* **138**, 9183−9192 (2016).
36. Han, G. Q. et al. Visible-light-driven valorization of biomass intermediates integrated with H_2 production catalyzed by ultrathin Ni/CdS nanosheets. *J. Am. Chem. Soc.* **139**, 15584−15587 (2017).
37. Xie, S. J. et al. Visible light-driven C−H activation and C–C coupling of methanol into ethylene glycol. *Nat. Commun.* **9**, 1181, (2018).
38. Wu, B. G. et al. Ultrathin porous carbon nitride bundles with an adjustable energy band structure toward simultaneous solar photocatalytic water splitting and selective phenylcarbinol oxidation. *Angew. Chem. Int. Ed.* **60**, 4815–4822 (2021).
39. Li, X. B. et al. Mechanistic insights into the interface-directed transformation of thiols into disulfides and molecular hydrogen by visible-light irradiation of quantum dots. *Angew. Chem. Int. Ed.* **53**, 2085–2089 (2014).
40. Liu, H., Xu, C. Y., Li, D. D. & Jiang, H.-L. Photocatalytic hydrogen production coupled with selective benzylamine oxidation over mof composites. *Angew. Chem. Int. Ed.* **57**, 5379–5383 (2018).
41. Wu, W. M. et al. Highly efficient visible-light-induced photocatalytic hydrogenation of nitrobenzene to aniline in water. *RSC Adv.* **3**, 10894–10899 (2013).
42. Li, M. Q. et al. PdPt alloy nanocatalysts supported on TiO_2: Maneuvering metal–hydrogen interactions for light-driven and water-donating selective alkyne semihydrogenation. *Small* **13**, 1604173 (2017).
43. Fan, X., Yao, Y. L., Xu, Y. S., Yu L. & Qiu, C. T. Visible-light-driven photocatalytic hydrogenation of olefins using water as the H source. *ChemCatChem* **11**, 2596–2599 (2019).
44. Han, C. H. et al. Beyond hydrogen evolution: solar driven water-donating transfer hydrogenation over platinum/carbon nitride. *ACS Catal.* **10**, 9227–9235 (2020).
45. Liu, C. B. et al. Controllable deuteration of halogenated compounds by photocatalytic D_2O splitting. *Nat. Commun.* **9**, 80 (2018).
46. Ling, X. et al. A visible-light-photocatalytic water-splitting strategy for sustainable hydrogenation/deuteration of aryl chlorides. *Sci. China Chem.* **63**, 386–392 (2020).
47. Gong, X. C. et al. Ligand-free palladium catalyzed Ullmann biaryl synthesis: "household' reagents and mild reaction conditions. *Green Chem.* **21**, 995–999 (2019).
48. Wang, Z. J. et al. Nondirecting group sp^3 C-H activation for synthesis of bibenzyls via homo-coupling as catalyzed by reduced graphene oxide supported PtPd@Pt porous nanospheres. *Adv. Synth. Catal.* **360**, 932–941 (2018).
49. Wang, L., Yuhong Zhang, Y. H., Liu, L. F. & Wang, Y. G. Palladium-catalyzed homocoupling and cross-coupling reactions of aryl halides in poly(ethylene glycol). *J. Org. Chem.* **71**, 1284–1287 (2006).
50. Mao, R. L. et al. Synthesis of C-mannosylated glycopeptides enabled by Ni-catalyzed photoreductive cross-coupling reactions. *J. Am. Chem. Soc.* **143**, *32*, 12699–12707 (2021).
51. Sheng, J. et al. Diversity-oriented synthesis of aliphatic fluorides via reductive C(sp3)−C(sp3) cross-coupling fluoroalkylation. *Angew. Chem. Int. Ed.* **60**, 15020–15027 (2021).
52. Miranda-Pizarro, J. et al. Reductive C–C coupling from molecular Au(I) hydrocarbyl complexes: a mechanistic study. *J. Am. Chem. Soc.* **143**, *32*, 2509–2522 (2021).
53. Kim, S., Goldfogel, M. J., Gilbert, M. M., & Weix. D. J. Nickel-catalyzed cross-electrophile coupling of aryl chlorides with primary alkyl chlorides. *J. Am. Chem. Soc.* **142**, *32*, 9902−9907 (2020).
54. Jiao, K.-J. et al.Nickel-catalyzed electrochemical reductive relay cross-coupling of alkyl halides to

aryl halides. *Angew. Chem. Int. Ed.* **59**, 6520–6524 (2020).
55. Sakai, H. A., Liu, W., Le, C. C. & MacMillan W. C. D. Cross-electrophile coupling of unactivated alkyl chlorides. *J. Am. Chem. Soc.* **142**, *32*, 11691−11697 (2020).
56. Chmiel, A. F., Williams, O. P., Chernowsky, C. P., Yeung, C. S. & Wickens, Z. K. Non-innocent radical ion intermediates in photoredox catalysis: parallel reduction modes enable coupling of diverse aryl chlorides. *J. Am. Chem. Soc.* **143**, *32*, 10882−10889 (2021).
57. Zhao, D. M. et al. Boron-doped nitrogen-deficient carbon nitride-based Z-scheme heterostructures for photocatalytic overall water splitting. *Nat. Energy* **6**, 388–397 (2021).
58. Li, Y. R. et al. Single-atom nickel terminating sp^2 and sp^3 nitride in polymeric carbon nitride for visible-light photocatalytic overall water splitting. *Chem. Sci.* **12**, 3633–3643 (2021).
59. Zhang, D. L. et al. Polymeric carbon nitride-derived photocatalysts for water splitting and nitrogen fixation. *Small* **17**, 2005149 (2021).
60. Qin, J. N. et al. Direct growth of uniform carbon nitride layers with extended optical absorption towards efficient water-splitting photoanodes. *Nat. Commun.* **11**, 4701 (2020).
61. Lin, Y., Su, W. Y., Wang, X. X., Fu, X. Z. & Wang, X. C. LaOCl-coupled polymeric carbon nitride for overall water splitting through a one-photon excitation pathway. *Angew. Chem. Int. Ed.* **59**, 20919 – 20923 (2020).
62. Li, G. X. et al. Phosphorus-doped iron nitride nanoparticles encapsulated by nitrogen-doped carbon nanosheets on iron foam in situ derived from saccharomycetes cerevisiae for electrocatalytic overall water splitting. *Small* **16**, 2001980 (2020).
63. Lin, L. H. et al. Molecular-level insights on the reactive facet of carbon nitride single crystals photocatalysing overall water splitting. *Nat. Caltal.* **6**, 388–397 (2021).
64. Kranz, C. & Wachtler, M. Characterizing photocatalysts for water splitting: from atoms to bulk and from slow to ultrafast processes. *Chem. Soc. Rev.* **50**, 1407–1437 (2021).
65. Wang, Z., Li C. & Domen, K. Recent developments in heterogeneous photocatalysts for solar-driven overall water splitting. *Chem. Soc. Rev.* **48**, 2109-2125 (2019).
66. Guo, Y. et al. Selectively catalytic hydrogenation of styrene-butadiene rubber over Pd/g-C_3N_4 catalyst. *Appl. Catal. A: Gen.* **589**, 117312 (2020).

Acknowledgements

The authors would like to thank the Key R & D and promotion projects in Henan Province (Grant No. 212102310372), the Natural Science Foundation of Henan Province (Grant No. 212300410358) and the financial supports from the National Natural Science Foundation of China (Grant No. 21603060).

Author contributions

X. T., Y. G., W. L. and Y. Z. performed the experiments. Y.-L. R., X. T. and Y. G. wrote the paper. Y.-L. R., Y. G., W. L. conducted the data analysis. Y.-L. R., X. T., W. A., C. N. and J. W. conceived the project. All authors discussed the results and commented on the paper.

Competing interests

The authors declare no competing interests.

Additional information

Supplementary information The online version contains supplementary material available at https://doi.org/

Correspondence and requests for materials should be addressed to Y.-L. R. or J.W.

Supplementary Files

This is a list of supplementary files associated with this preprint. Click to download.

- SupportingInformation.pdf